

Nonlinear interaction of head-on solitary waves in integrable and nonintegrable systems

Shutian Zhang(张树甜), Shikun Liu(刘世鲲), Tengfei Jiao(矫滕菲), Min Sun(孙敏), Fenglan Hu(胡凤兰), and Decai Huang(黄德财)

Citation: Chin. Phys. B, 2024, 33 (**5**): 054501. DOI: 10.1088/1674-1056/ad1dcb
Journal homepage: http://cpb.iphy.ac.cn; http://iopscience.iop.org/cpb

What follows is a list of articles you may be interested in

Decaying solitary waves propagating in one-dimensional damped granular chain

Zongbin Song(宋宗斌), Xueying Yang(杨雪滢), Wenxing Feng(封文星), Zhonghong Xi(席忠红), Liejuan Li(李烈娟), Yuren Shi(石玉仁)
Chin. Phys. B, 2018, 27 (**7**): 074501. DOI: 10.1088/1674-1056/27/7/074501

Head-on collision between two solitary waves in a one-dimensional bead chain

Fu-Gang Wang(王扶刚), Yang-Yang Yang(杨阳阳), Juan-Fang Han(韩娟芳), Wen-Shan Duan(段文山)
Chin. Phys. B, 2018, 27 (**4**): 044501. DOI: 10.1088/1674-1056/27/4/044501

Envelope solitary waves and their reflection and transmission due to impurities in a granular material

Wen-Qing Du(杜文青), Jian-An Sun(孙建安), Yang-Yang Yang(杨阳阳), Wen-Shan Duan(段文山)
Chin. Phys. B, 2018, 27 (**1**): 014501. DOI: 10.1088/1674-1056/27/1/014501

Biphasic behavior of energy in a stepped chain

Ping-Jian Wang(王平建), Ai-Xiang He(何爱香), Zhong-Hai Lin(林忠海), Guang-Fen Wei(魏广芬), Yan-Li Liu(刘燕丽)
Chin. Phys. B, 2016, 25 (**6**): 064501. DOI: 10.1088/1674-1056/25/6/064501

Binary collision approximation for solitary waves in a Y-shaped granular chain

Chen Qiong (陈琼), Yang Xian-Qing (杨先清), Zhao Xin-Yin (赵新印), Wang Zhen-Hui (王振辉), Zhao Yue-Min (赵跃民)
Chin. Phys. B, 2013, 22 (**1**): 014501. DOI: 10.1088/1674-1056/22/1/014501

Nonlinear interaction of head-on solitary waves in integrable and nonintegrable systems

Shutian Zhang(张树甜), Shikun Liu(刘世鲲), Tengfei Jiao(矫滕菲), Min Sun(孙敏), Fenglan Hu(胡凤兰), and Decai Huang(黄德财)†

Department of Applied Physics, Nanjing University of Science and Technology, Nanjing 210094, *China*

(Received 27 October 2023; revised manuscript received 4 January 2024; accepted manuscript online 12 January 2024)

This study numerically investigates the nonlinear interaction of head-on solitary waves in a granular chain (a nonintegrable system) and compares the simulation results with the theoretical results in fluid (an integrable system). Three stages (the pre-in-phase traveling stage, the central-collision stage, and the post-in-phase traveling stage) are identified to describe the nonlinear interaction processes in the granular chain. The nonlinear scattering effect occurs in the central-collision stage, which decreases the amplitude of the incident solitary waves. Compared with the leading-time phase in the incident and separation collision processes, the lagging-time phase in the separation collision process is smaller. This asymmetrical nonlinear collision results in an occurrence of leading phase shifts of time and space in the post-in-phase traveling stage. We next find that the solitary wave amplitude does not influence the immediate space-phase shift in the granular chain. The space-phase shift of the post-in-phase traveling stage is only determined by the measurement position rather than the wave amplitude. The results are reversed in the fluid. An increase in solitary wave amplitude leads to decreased attachment, detachment, and residence times for granular chains and fluid. For the immediate time-phase shift, leading and lagging phenomena appear in the granular chain and the fluid, respectively. These results offer new knowledge for designing mechanical metamaterials and energy-mitigating systems.

Keywords: integrable system, nonintegrable system, granular chain, solitary wave

PACS: 45.70.–n, 47.35.Fg, 05.45.–a, 04.60.Nc **DOI:** 10.1088/1674-1056/ad1dcb

1. Introduction

Nonlinear waves have been observed extensively in nature, such as in oceans, plasmas, solid lattices, biological molecules and optical systems.[1–6] A solitary wave (SW) is unique because of its localization and stabilization properties.[7,8] The classical Korteweg–de Vries (KdV) equation, which is integrable, was first introduced to describe the traveling dynamics of SW in shallow water.[9] The other known integrable equations have analytical SW solutions, such as the sine-Gordon equation and the nonlinear Schrödinger equation.[7] However, many nonlinear systems admitting solitary waves (SWs), such as the granular chain (GC) system and the Fermi–Pasta–Ulam–Tsingou system, are nonintegrable.[10–13] In general, a SW with higher amplitude has a larger wave speed for integrable and nonintegrable systems. For the former, increasing the amplitude of SWs can decrease their width.[7] For the latter, Nesterenko first found the existence of SWs in a sonic-vacuum GC whose width was independent of the wave amplitude.[14] Following his pioneering work, a large number of activities involving SWs in GC systems have been focused on the excitation of SWs, the reflection and transmission of SWs at an interface, and the interaction of SWs.[15–31] Therefore, comparing the traveling dynamics between integrable and nonintegrable systems is of great significance.

Given the intrinsic characteristics of the interaction between the touching grains in GC systems, such as Hertzian force for spherical grains, the key difference is reflected in the interactions between the SWs compared with those in integrable systems. Experimental and numerical studies play a great role because of the nonintegrability of the constitutive equations.[16–18] To create a SW in a GC, a commonly used method is an instantaneous impulse imparted on the sidemost grain. Sen *et al.* found that the central grain remains static in an odd chain, and oscillatory motions of the grains around the center are observed, which leads to the formation of secondary SWs.[19–21] The occurrence of secondary SWs was confirmed by experimental results.[23] To compare the difference between the collisions of SWs in integrable and nonintegrable systems, Shen *et al.* directly introduced the analytical solutions of SWs of the KdV equation and Toda lattice into the GC.[24] In the integrable systems, the nonlinear collision effect is observed, which leads to a phase shift appearing though the SWs after the collision recover the amplitude and propagation velocity of the incident SWs. The phase shift is also observed in a nonintegrable GC system owing to a nonlinear collision. However, the nonlinear scattering effect occurs, leading to the generation of secondary SWs, and the amplitude of the SWs decreases after the collision. Whether a phase shift is generated is still a controversial issue. Wang *et al.* employed the KdV solution as the incident waves to study the collision dynamics of head-on propagating solitary waves (HSWs) in

†Corresponding author. E-mail: hdc@njust.edu.cn

© 2024 Chinese Physical Society and IOP Publishing Ltd

a GC.[25] The simulation results indicated that the collision of the HSWs does not influence the waveform and amplitude, and no phase shift happens. In our previous study, the phase shift arose after HSWs collided in a GC when the analytical SW solution of the Toda lattice was used for incident SWs.[26] Further results show that the collision of HSWs can be divided into two processes: early incident collision and later separation collision processes. Lagging and leading phases are discovered, respectively. The latter's effect is stronger than the former, resulting in a leading phase after the collision.

The collision dynamics of HSWs is also a critical topic in integrable systems.[32–38] Taking continuous fluid as an example, Su *et al*. carried out a third-order perturbation analysis on the collisions of HSWs.[32] They found that an increase in the amplitude of HSWs increases the immediate space-phase shift (at the collision center) and the uniform space-phase shift (far away from the collision center). When the HSWs are two identical SWs, the collision dynamics of HSWs is found to be equivalent to that of a single SW and a vertical wall.[37–42] Cooker *et al*. explored the time-phase shift by introducing the definitions of the attachment, detachment, and residence times.[41] The results show that these characteristic times decrease with an increased amplitude of HSWs. Similar results were reproduced in integrable plasma systems.[43–45] For the collision of two identical HSWs, analytical and simulated results evidenced that increasing wave amplitude can increase space-phase shift. The reported results have shown that the collision dynamics of HSWs share a common characteristic, that is, phase shift, in integrable and nonintegrable systems. The SWs after the collision can recover their initial incident waveform for the former. For the latter, the scattering effect due to the nonlinear collision leads to secondary SWs, and the amplitude of the SWs decreases after the collision. Therefore, borrowing the theoretical analysis methods used in integrable systems to describe the collision dynamics of HSWs in nonintegrable granular chains (GCs) is of great significance.

This study explores the nonlinear interaction of two identical HSWs in a nonintegrable sonic-vacuum GC. The complex collision process is elucidated using the theoretical analysis method in fluid. The structure of this study is as follows: Section 2 sets up the simulation model for an unprecompressed GC, Section 3 revisits the theoretical analysis of the collision of HSWs in a GC and fluid, Section 4 presents the simulation results and compares them with those in fluid (i.e., space-phase shift and time-phase shift), and Section 5 draws our conclusions.

2. Simulation model

The discrete element method is used to explore the collision characteristics of HSWs in a one-dimensional monodisperse GC comprised of N spherical elastic beads with mass m and radius R. The interaction between two neighboring beads, without dissipation, is modeled by the Hertz potential[46]

$$U = \begin{cases} \frac{2}{5}k\delta^{5/2}, & \delta \geq 0, \\ 0, & \delta < 0, \end{cases} \tag{1}$$

where δ is the overlap deformation between touching beads and $k = E\sqrt{2R}/[3(1-\sigma^2)]$ is the elastic coefficient, which reflects the material and geometric properties of the beads. E and σ are the Young's modulus and Poisson ratio, respectively. In the simulation, an unprecompressed GC is considered, which is always called a sonic-vacuum GC. For the touching beads, the equation of motion for bead i is given by

$$m\ddot{s}_i = k\left[(s_{i-1}-s_i)^{3/2} - (s_i - s_{i+1})^{3/2}\right]. \tag{2}$$

Overdots denote time derivatives, and s_i is the displacement of bead i from its equilibrium position.

In a simulation time step, the velocity Verlet algorithm is used to solve Eq. (2). The integration time step is 10^{-8} s. In each simulation run, the ratio of the instantaneous total energy to the initial total energy is monitored, which fluctuates at the order of magnitude of 10^{-10}. Smaller time steps cannot make any significant improvement in the calculation accuracy of numerical simulations. The material of the beads is stainless steel, and its parameters are as follows: Young's modulus $E = 200$ GPa, Poisson's ratio $\sigma = 0.28$, density $\rho = 7.9 \times 10^3$ kg/m^3, radius $R = 2.5$ mm. The number of beads is $N = 400$.

To produce a SW, the leftmost bead of the GC is set to an impulse velocity v_0 and the others are zero.[16–18] The incident impulse spreads in the GC after a certain traveling distance, composed of a leading single right-traveling solitary wave (RSW) and a train of following secondary waves. This study examines the collision of HSWs by symmetrically placing two identical SWs at the sides of bead 200, the centers of which are located at bead 101 and bead 299, respectively. They are named the right-traveling scattered solitary wave (RSSW) and the left-traveling scattered solitary wave (LSSW), as shown in Fig. 1. The collision center of the HSWs is located at bead 200 because of the identical symmetry of the RSSW and LSSW. The study introduces t_i as the arrival time when the contact force F_i between bead i and bead $i+1$ reaches the maximum, which is normalized by $(k/m)^{-1/2}(2R)^{-1/4}$.

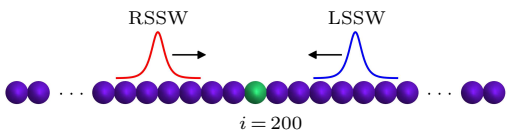


Fig. 1. Schematic view of the simulation model. The collision center is located at bead 200, which is green. The red and blue solid lines are for the right- and left-traveling scattered solitary waves, respectively. The arrows stand for the traveling direction of the solitary waves.

3. Theoretical analysis

In Nesterenko's considerations, a theoretical solution of SWs is suggested using the long-wavelength approximation.[10] Keeping terms up to the fourth order in spatial derivatives for Eq. (2), a continuous equation is derived using the strain $\xi = -s_x$,[14]

$$\xi_{tt} = c^2 \left\{ \xi^{3/2} + \frac{R^2}{3} \left[\left(\xi^{3/2} \right)_{xx} - \frac{3}{8} \left(\xi^{-1/2} \right) \xi_x^2 \right] \right\}_{xx},$$
$$\xi > 0, \quad c^2 = \frac{2E}{\pi\rho(1-\sigma^2)} = \frac{k}{m} (2R)^{5/2}. \tag{3}$$

The constant c is of the same order of magnitude as the bulk sound speed in the grains. A single hump of periodic solution of Eq. (3) with a fixed width of five bead diameters describes the proposed SW solution

$$\xi = \left(\frac{5V_s^2}{4c^2} \right)^2 \cos^4 \left(\frac{x - V_s t}{\sqrt{10}R} \right), \tag{4}$$

where x is the laboratory coordinate and V_s is the SW speed with a nonlinear dependence on the maximum bead velocity v_m,[10,14,47]

$$V_s = \left(\frac{16}{25} \right)^{1/5} c^{4/5} v_m^{1/5} = 2R \left(\frac{4k}{5m} \right)^{2/5} v_m^{1/5}. \tag{5}$$

Considering the spatial compactness of a single SW, the quasi-particle model with $1.4m$ in mass and $1.4v_m$ in velocity has frequently been introduced to describe its dynamics.[14,48–51] For the collision of two identical HSWs, one SW is regarded as static and approached by the other at the velocity of twice $1.4v_m$. According to elastic theory, the time-phase difference is determined by the collision duration time of a single SW colliding with a static one, minus the duration time of the nonlinear collision of two identical HSWs,[46]

$$\Delta t_G = 0.4 \left(\frac{5\sqrt{2}\pi\rho}{4} \frac{1-\sigma^2}{E} \right)^{2/5} \frac{R}{v_m^{1/5}}$$
$$= 0.4 \left(\frac{5m}{8k} \right)^{2/5} v_m^{-1/5}. \tag{6}$$

For comparison purposes, we briefly revisit the nonlinear collision characteristics of HSWs as described by the classical KdV equation in shallow water, which has been analytically solved,[52,53]

$$\pm\eta_t + \left(1 + \frac{3}{2}\alpha\eta \right) \eta_x + \frac{\beta^2}{6} \eta_{xxx} = 0,$$
$$\alpha = \frac{A_0}{h}, \quad \beta = k_0 h, \tag{7}$$

where x, t, and η are the dimensionless horizontal coordinate, time, and free surface displacement. A_0 and k_0 are the characteristic wave amplitude and wave number, and h is the water depth. Equation (7) has an exact analytical solution in the SW form

$$\eta = \operatorname{sech}^2 \left\{ \frac{\sqrt{3\alpha}}{2\beta} \left[x \mp \left(1 + \frac{\alpha}{2} \right) t \right] \right\}, \tag{8}$$

where the upper and lower signs denote the right- and left-traveling SWs in Eqs. (7) and (8).

The reflection of a single SW at a vertical wall is equivalent to the nonlinear collision of two identical HSWs in fluid.[37–42] Similarly, such considerations are also used in studies of the collision of HSWs in GCs.[19,20] Compared with traveling a single SW, the collision of two HSWs in fluid leads to a space-phase shift. When the two pieces of HSWs move away from each other, the uniform space-phase shift is theoretically derived using third-order approximation[32]

$$\Delta x_{\mathrm{Un,R}} = \left(\frac{A_L}{3} \right)^{1/2} \left(1 + \frac{1}{8}A_L + \frac{3}{4}A_R \right), \tag{9a}$$
$$\Delta x_{\mathrm{Un,L}} = -\left(\frac{A_R}{3} \right)^{1/2} \left(1 + \frac{1}{8}A_R + \frac{3}{4}A_L \right). \tag{9b}$$

At the position of the collision center, the phase shift in space occurs, defined as an immediate space-phase shift,

$$\Delta x_{\mathrm{Im,R}} = \left(\frac{A_L}{3} \right)^{1/2} \left(1 + \frac{1}{8}A_L + \frac{23}{4}A_R \right), \tag{10a}$$
$$\Delta x_{\mathrm{Im,L}} = -\left(\frac{A_R}{3} \right)^{1/2} \left(1 + \frac{1}{8}A_R + \frac{23}{4}A_L \right). \tag{10b}$$

The space-phase shift Δx and wave amplitude A are reduced by the water depth h. The subscripts R and L denote the right- and left-traveling SWs, respectively.

For the collision of a single SW with a static wall, two characteristic times, that is, the attachment time $\Delta t_a = t_a - t_0$ and the detachment time $\Delta t_d = t_d - t_0$, are two critical physical quantities describing the collision dynamics. t_a and t_d are when the incident wave crest arrives and leaves the wall, respectively. Under perfect reflection, the reflection is completed instantaneously, meaning that t_a and t_d collapse together. This moment is the reference time point t_0.[35,42] The characteristic times can be written as[41]

$$\Delta t_a = t_a - t_0 = \frac{2}{\sqrt{3}} \left(-\kappa A^{-1/2} + \frac{1}{8}(2-\kappa) A^{1/2} \right), \tag{11a}$$
$$\Delta t_d = t_d - t_0 = \frac{2}{\sqrt{3}} \left(\kappa A^{-1/2} + \frac{1}{8}(2+\kappa) A^{1/2} \right). \tag{11b}$$

Using the attachment time Δt_a and detachment time Δt_d, the residence time $\Delta t_r = t_d - t_a$ is introduced to describe the duration of the collision,

$$\Delta t_r = t_d - t_a = \frac{4\kappa}{\sqrt{3}} \left(A^{-1/2} + \frac{1}{8} A^{1/2} \right), \tag{12}$$

where $\kappa = \tanh^{-1}\left(1/\sqrt{3}\right)$. The turning time t_0' is also directly derived, which indicates the change time from the incident

wave to the reflected wave. For the collision of two identical HSWs, the maximum collision force appears at the time of t_0'. The time difference of $t_0' - t_0$ is the immediate time-phase shift at the position of the collision center of the HSWs,

$$\Delta t_{\rm Im} = t_0' - t_0 = \frac{1}{2\sqrt{3}}\left(A^{1/2} + \frac{43}{8}A^{3/2}\right). \tag{13}$$

The time is normalized by $\sqrt{h/g}$, and g is the acceleration due to gravity.

4. Simulation results and discussion

4.1. Dynamics of head-on collision

The time evolution of a single RSW and two pieces of HSWs when the maximum collision forces reach beads 150, 190, 200, 210, 250, and 300 is plotted in Fig. 2 to understand the collision dynamics of HSWs in a GC. In each simulation run, the amplitude of the maximum force of the RSW fluctuates slightly. In Fig. 2, the maximum forces and arrival times of the RSSW and LSSW are completely symmetrical about the central bead of 200. Thus, the following comparisons are only performed on the results of the RSW and RSSW.

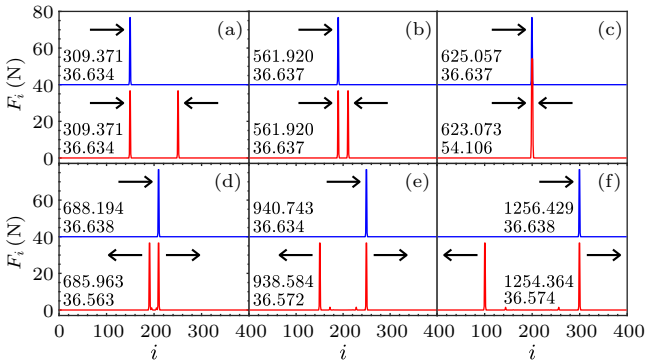


Fig. 2. Collision force as a function of bead number for a single right-traveling solitary wave (blue lines) and head-on propagating solitary waves (red lines) with impact velocity $v_0 = 1$ m/s. Panels (a)–(f) show snapshots of when the maximum forces reach beads 150, 190, 200, 210, 250, and 300, and the corresponding arrival times are recorded. The data for the single right-traveling solitary wave are shifted by 40 N. The arrows stand for the traveling direction of the solitary waves.

The simulation results indicate three traveling stages of the two pieces of HSWs, namely, the pre-in-phase traveling stage (pre-RSSW/pre-LSSW), the central-collision stage, and the post-in-phase traveling stage (post-RSSW/post-LSSW). At the pre-in-phase traveling stage, the RSSW travels freely in the GC because the collision has not occurred yet. The maximum force and arrival time of the RSSW are equal to those of the RSW shown in Figs. 2(a) and 2(b). When the central-collision stage occurs, a clear nonlinear superposition of the two pieces of HSWs is observed in Fig. 2(c), in which the collision reaches its central point, bead 200. The collision between the HSWs yields a maximum force of 54.106 N, which is less than twice that of the RSW. Furthermore, the collision decreases the arrival time for the RSSW (623.073), as contrasted with the RSW (625.057). The leading-time phase equals -1.984, which is just the immediate time-phase shift. When the centers of two pieces of HSWs pass through each other, the arrival time of the RSSW is smaller than that of the RSW, as shown in Figs. 2(d), 2(e) and 2(f). The former are 685.963, 938.584, and 1254.364 for beads 210, 250, and 300, respectively. The corresponding latter are 688.194, 940.743, and 1256.429, respectively. With increased separation distance between the centers of the RSSW and LSSW, the two pieces of HSWs stop interacting and reach the stable post-in-phase traveling stage. In this stage, as shown in Figs. 2(e) and 2(f), the arrival time difference between the RSSW and the RSW becomes a constant value. The leading-time phase in the former is -2.159 and that in the latter is -2.065. In addition, two symmetrical secondary waves with tiny magnitudes are observed, which have about 0.3% the energy of pre-RSSW and pre-LSSW. An increase in calculation accuracy, such as time step 10^{-9} s, cannot influence the lost energy stored in the secondary waves.

Based on the discussion of the three traveling stages, the final leading-time phase is generated in the central collision stage. To explore the collision dynamics of this stage, the arrival time is plotted as a function of the bead number around bead 200, as depicted in Fig. 3. The arrival times of the RSW and RSSW for beads 198 to 207 are given in Table 1. The absolute value of Δt_i becomes larger from beads 202 to 207, but the absolute value of $\Delta t_i - \Delta t_{i-1}$ decreases. The difference between Δt_{207} and Δt_{206} is less than 10^{-2}, which implies the central-collision stage is finished and the stable post-in-phase traveling stage starts. As shown in Table 1, the central-collision stage has an eight-bead width, namely, $199 \le i \le 206$, for RSSW. Then the simulation results are fitted using the least-square method, $x_j^+ = a_j^+ t + b_j^+$ for the pre-in-phase traveling stage ($i < 199$ for pre-RSSW or $i > 201$ for pre-LSSW) and $x_j^- = a_j^- t + b_j^-$ for the post-in-phase traveling stage ($i > 206$ for post-RSSW or $i < 194$ for post-LSSW), respectively, where the subscripts $j = \mathrm{R}, \mathrm{L}$ represent the traveling direction of the SWs. The fitting functions are $x_{\rm R}^+ = 0.158385t + 101.00$ and $x_{\rm R}^- = 0.158340t + 101.38$ for pre-RSSW and post-RSSW, respectively, in which the fitted propagation velocities agree well with those of Eq. (5) (0.159631 for pre-RSSW and 0.159584 for post-RSSW). The propagation velocity of pre-RSSW is expected to be equal to that of RSW, whereas the post-RSSW's propagation velocity decreases owing to the collision of HSWs. The initial-space phase of $x_{\rm R}^+$ is 101.00 consistent with the beginning location of the RSSW. The initial-space phase of post-RSSW, 101.38, is obtained from the fitting result, and the leading-space phase is 0.38. Similarly, the same fitting method is used for the LSSW, leading to symmetrical results of $x_{\rm L}^+ = -0.158385t + 299.00$ and $x_{\rm L}^- = -0.158340t + 298.62$ for pre-LSSW and post-LSSW,

respectively. The collision of HSWs causes a decrease in the propagation velocity of LSSW. However, the initial-space phase, 298.62, is also obtained for post-LSSW, smaller than the initial-space phase of pre-LSSW, 299.00. The corresponding leading-space phase is −0.38, consistent with the result for RSSW.

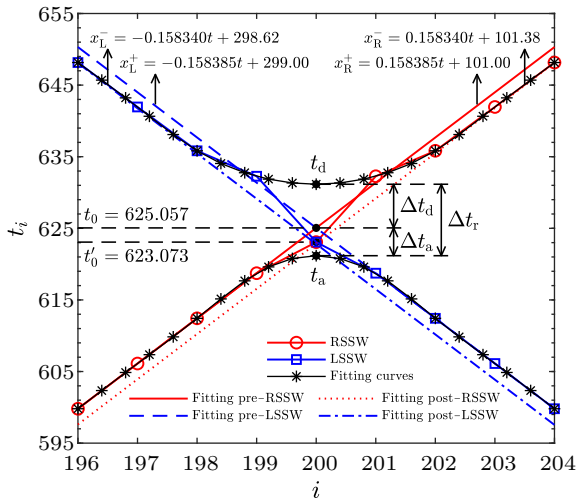


Fig. 3. The arrival time as a function of bead number near bead 200. The same parameters are used as in Fig. 2. The red circles and blue squares are for the trajectories of right- and left-traveling scattered solitary waves, respectively. The fitting straight lines are obtained using the least-square method, in which the red solid and blue dashed lines are for the right- and left-traveling scattered solitary waves in the pre-in-phase traveling stage, respectively. The red dotted and blue dash-dotted lines are for the right- and left-traveling scattered solitary waves in the post-in-phase traveling stage, respectively. t_0 and t_0' denote the simulation arrival times of bead 200 for single right-traveling solitary wave and head-on propagating solitary waves, respectively. The fitting curves are obtained by the third-order spline difference method, in which the lower and upper curves are for the incident and reflection parts for the interaction of a solitary wave with a vertical wall, respectively. t_a and t_d are the vertices of two fitting curves, and Δt_a and Δt_d represent the attachment and detachment times, respectively.

Table 1. The arrival times of single right-traveling solitary wave and right-traveling scattered solitary wave for beads 198 to 207.

i	$t_{i,\mathrm{RSW}}$	$t_{i,\mathrm{RSSW}}$	$\Delta t_i = t_{i,\mathrm{RSSW}} - t_{i,\mathrm{RSW}}$	$\Delta t_i - \Delta t_{i-1}$
198	612.430	612.430	0	
199	618.743	618.732	−0.011	−0.011
200	625.057	623.073	−1.984	−1.973
201	631.371	632.271	0.900	2.884
202	637.685	635.826	−1.859	−2.759
203	643.998	641.946	−2.052	−0.193
204	650.312	648.153	−2.159	−0.107
205	656.626	654.422	−2.204	−0.045
206	662.939	660.718	−2.221	−0.017
207	669.253	667.025	−2.228	−0.007

In Fig. 3, an asymmetrical characteristic of the central-collision stage is exhibited concerning bead 200 for HSWs. The simulation arrival times of RSSW for beads 199 and 200 are less than those for RSW, which means the occurrence of the leading-time phase. Conversely, the arrival time of RSSW for bead 201 is unexpectedly extended compared with that of RSW, which means a lagging-time phase. For bead 202 and the latter beads of RSSW, a leading-time phase reappears, in which the arrival time of RSSW is less than that of RSW. Thus, the central-collision stage can be divided into two sub-stages (i.e., the incident collision process and the separation collision process). The former exhibits a compression process and the latter an expansion process. The leading-time phase covers the entire compression process and the latter half of the expansion process, and the lagging-time phase only appears in the first half of the expansion process. This collision characteristic is the reverse of our previous observations for the collision of HSWs, which may be due to the different systems selected (the system in Ref. [26] is a compressed GC) or the different kinds of SWs (the incident SW in Ref. [26] is the SW solution of a Toda lattice). However, the leading-time phase is more prominent than the lagging-time phase. A leading phase shift of time occurs for the HSWs after the collision, consistent with that in a compressed GC.

4.2. Space-phase shift

From the observations presented above, the nonlinear collision of HSWs leads to leading phase shifts in time and space though the amplitude of the propagation velocity of SWs decreases after the collision. To compare the space-phase shift of HSWs in nonintegrable GCs and integrable fluid, we employ the same analysis method used in fluid to obtain fitting functions for pre-in-phase and post-in-phase traveling stages.[54] The immediate space-phase shift at the collision center is calculated by the difference in the intercepts of the fitting lines at the arrival time of maximum collision force t_0',

$$\Delta x_{\mathrm{Im},j} = \left(a_j^- - a_j^+\right) t_0' + \left(b_j^- - b_j^+\right), \quad j = \mathrm{R}, \mathrm{L}. \tag{14}$$

The fitting results of RSSW and LSSW in Fig. 3 give the same immediate space-phase shifts (i.e., $\Delta x_{\mathrm{Im,R}} = 0.3562$ and $\Delta x_{\mathrm{Im,L}} = -0.3562$).

We also conducted a series of similar simulations on the collisions of HSWs with different amplitudes normalized by $2R$. The immediate space-phase shift of RSSW against the wave amplitude of HSWs is plotted in Fig. 4. Unexpectedly, the immediate space-phase shift in the GC remains constant at 0.3563, whereas a monotonic increase is found in fluid. This unique collision characteristic of HSWs in a GC can be reasonably explained using the quasi-particle arguments in Section 3. The immediate space-phase shift is the product of the propagation velocity, given by Eq. (5), and the time-phase difference, given by Eq. (6). The theoretical result is 0.3031, which does not depend on the wave amplitude of HSWs. Moreover, three stainless steel beads with $R = 1.25$ mm, 2.5 mm and 5 mm and one plexiglass bead with $R = 2.5$ mm are used in the simulations. All results fall on the same straight line, with an average of $\Delta\bar{x}_{\mathrm{Im,R}} = 0.3563$. The parameters of the plexiglass bead are as follows: Young's modulus $E = 71.7$ GPa, Poisson's ratio $\sigma = 0.23$, density $\rho = 2.5 \times 10^3$ kg/m^3, and radius $R = 2.5$ mm.[30]

Two determined factors for the space-phase shift after collision are the immediate space-phase shift at the collision center and the propagation velocity difference between RSW and post-RSSW. When the collision of HSWs occurs in fluid, the SWs can recover their original incident waveform after the collision.[32–34,38] The uniform space-phase shift given by Eq. (9) is only determined by the wave amplitude of HSWs, independent of the measurement position. However, for the case of the GC, as observed in Fig. 2, the nonlinear scattering effect in the central-collision stage leads to a decrease in the amplitude of post-RSSW compared with that of RSW. In Fig. 4, the results show that the wave amplitude of HSWs does not influence the immediate space-phase shift. On the other hand, the post-RSSW travels stably at a lower propagation velocity in the GC after the collision. Thus, the space-phase shift after the collision is expected to decrease linearly with an increase in the traveling distance of the post-RSSW, as confirmed by the simulation results shown in Fig. 5 for impact velocities of $v_0 = 0.1$ m/s, 1 m/s and 10 m/s.

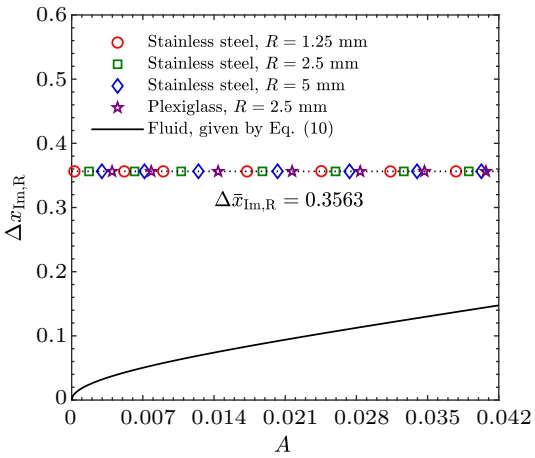


Fig. 4. Immediate space-phase shift of right-traveling scattered solitary wave as a function of the wave amplitude of head-on propagating solitary waves. The red circles, green squares, and blue diamonds are for the stainless steel beads with radii of 1.25 mm, 2.5 mm, and 5 mm, respectively. The purple pentagrams are for the plexiglass beads with a radius of 2.5 mm. The black solid line is for the immediate space-phase shift of fluid, given by Eq. (10).

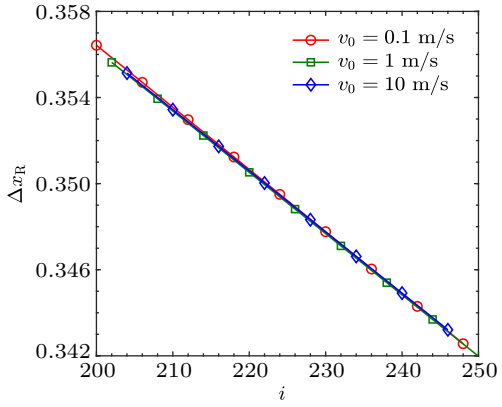


Fig. 5. Space-phase shift of right-traveling scattered solitary wave as a function of bead location. The stainless steel bead radius is 2.5 mm. The red circles, green squares, and blue diamonds are for impact velocities of 0.1 m/s, 1 m/s, and 10 m/s, respectively.

4.3. Collision characteristic time of HSWs

The above observations have demonstrated that the nonlinear scattering effect occurs in the central-collision stage for GCs and fluid. The space-phase shift of the former is independent of wave amplitude, whereas that of the latter increases with the wave amplitude of HSWs. For complete comparison purposes, we next compare the characteristic time of the central-collision stage for GCs and fluid. Theoretical results in fluid from Eqs. (11) and (12), as well as the fitting results in the GC, are shown in Figs. 6(a)–6(c). For the collision of HSWs in the GC, the collision center is located at bead 200 due to the symmetry of HSWs. Bead 200 stays stationary during the entire collision process and can be regarded as an infinite-mass bead at the center of a GC.[19,20] Similar to the fluid analysis, the arrival time of bead 200 for RSW is chosen as the reference time point t_0, which is the turning point between the incident and reflection waves in perfect reflection. The attachment and detachment times are also introduced for the GC using a similar analysis method to that in fluid (Eq. (11)) shown in Fig. 3. The third-order spline difference method is used to fit the curves to ensure that all the data except the result of bead 200 fall on the curves. The lower and upper curves represent the incident and reflection parts for the interaction of a SW with a vertical wall, respectively. t_{a} and t_{d} are the vertices of two fitting curves.

In Fig. 6(a), the attachment time Δt_{a} is plotted as a function of the wave amplitude of HSWs. Similar dependence is observed for the fitting results in the GC and the theoretical results in fluid predicted by Eq. (11a), both of which are negative values. Compared with perfect reflection, RSSW has a larger propagation velocity, resulting in an earlier arrival time at bead 200. Figure 6(b) plots the dependence of the detachment time Δt_{d} on the wave amplitude of HSWs. Similar results are observed for the GC and fluid, which are positive values. RSSW has a larger detachment time compared with the perfect reflection. In Fig. 6(c), the dependence of residence time Δt_{r} on the wave amplitude of HSWs is plotted, which is the time difference between t_{d} and t_{a}. The larger amplitude of HSWs decreases monotonically the residence time in the GC and fluid.

In Fig. 6(d), we plot the dependence of the immediate time-phase shift Δt_{Im} on the wave amplitude of HSWs for the GC and fluid. The reference time point is also placed at the turning point of perfect reflection, as for those in Figs. 6(a) and 6(b). The negative and positive values of Δt_{Im} denote that the collision of HSWs leads to the leading- and lagging-time phases, respectively. The smaller absolute value of Δt_{Im} means that the collision of the HSWs approaches the perfect reflection. As shown in Fig. 6(d), Δt_{Im} increases with an increase in the wave amplitude of HSWs for the GC and fluid. However, an unexpected opposite result is observed, i.e., Δt_{Im} for the GC is negative, whereas Δt_{Im} for fluid is positive. The collision of

HSWs in the GC approaches the perfect reflection as the wave amplitude of HSWs increases, while that for fluid is reversed. This opposite result may originate from the difference in research models: the GC model is a compressible Hertz system, whereas the fluid is assumed to be incompressible in previous studies.[32–35,38–42]

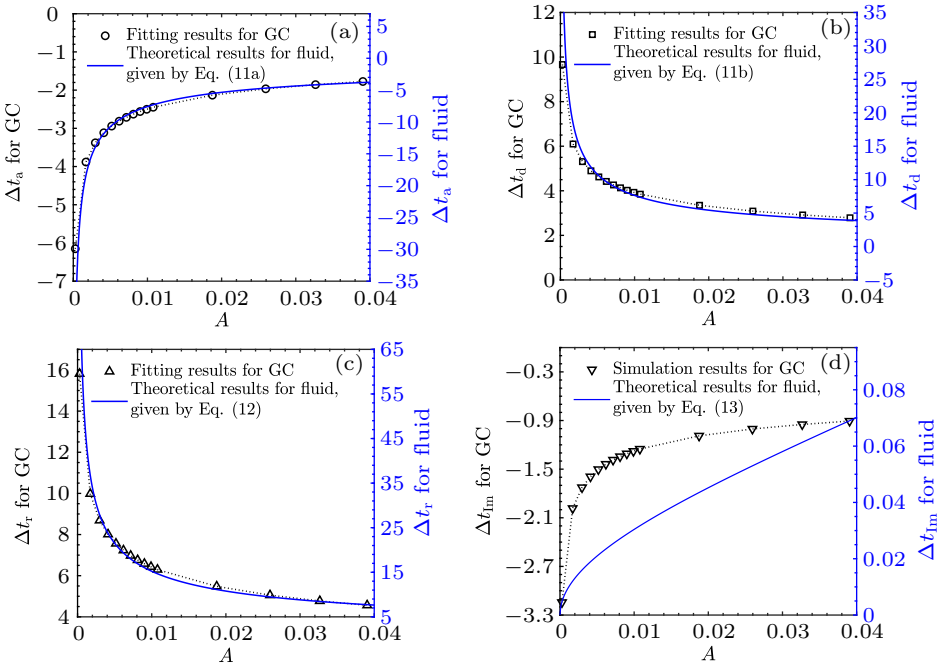


Fig. 6. Collision characteristic time as a function of the wave amplitude of head-on propagating solitary waves. The stainless steel bead radius is 2.5 mm. (a) Attachment time Δt_a; (b) detachment time Δt_d; (c) residence time Δt_r; (d) immediate time-phase shift Δt_{lm}. The black circles, squares, upward triangles, and downward triangles denote the results for the granular chain, respectively. The blue solid lines denote the theoretical results for fluid. The dotted lines are guides for the eyes.

5. Conclusions

In this study, the nonlinear interaction of two identical head-on solitary waves is numerically simulated in a sonic-vacuum granular chain, which is nonintegrable. The phenomenological solution of solitary waves proposed by Nesterenko is revisited, and the quasi-particle model is used to describe the collision of solitary waves. We also revisit the theoretical analysis of the classical Korteweg–de Vries equation in integrable fluid (i.e., phase shifts in space and time). Similar analyses are performed on the simulation results of granular chains, and the major findings are summarized as follows.

For the collision of head-on solitary waves in a granular chain, three stages are identified to describe the interaction processes: the pre-in-phase traveling stage, the central-collision stage, and the post-in-phase traveling stage. The solitary waves can travel freely in the pre-in-phase and post-in-phase traveling stages. The nonlinear scattering effect appears in the central-collision stage, leading to a decrease in the amplitude of solitary waves.

The central-collision stage has an asymmetrical collision characteristic, i.e., incident and separation collision processes, which correspond to the compression and expansion processes of solitary waves. In the entire compression process and the latter half of the expansion process, the leading-time phase occurs, and the lagging-time phase happens in the first half of the expansion process. The accumulation result leads to leading phase shifts in time and space after the collision of solitary waves.

In the granular chain, the immediate space-phase shift is found independent of wave amplitude and material parameters, which can be reasonably explained by the quasi-particle model. The space-phase shift after the collision is only determined by the measurement position rather than the wave amplitude. The corresponding results are reversed in fluid. In the former, the nonlinear scattering effect results in a decrease in the amplitude of solitary waves. The solitary waves recover their original incident waveform after the collision in the latter.

The attachment, detachment, and residence times decrease with the increasing amplitude of solitary waves for granular chains and fluid. However, the opposite result occurs for an immediate time-phase shift, i.e., a leading shift for granular chains and a lagging shift for fluid.

The present work lends insights into the nature of solitary wave interactions for nonintegrable granular chains by comparing the results with those of integrable fluid. This treatment provides a powerful analysis method to measure a variety of mechanical waves in integrable and nonintegrable systems accurately. The unique interaction properties of solitary waves in a granular chain stem from the special interaction between grains. These innovative observations pave the way to design-

ing energy-harvest and shock-protection devices.

Acknowledgements

Project supported by the National Natural Science Foundation of China (Grant No. 11574153) and the Foundation of the Ministry of Industry and Information Technology of China (Grant No. TSXK2022D007).

References

[1] Osborne A R and Burch T L 1980 *Science* **208** 451
[2] Shukla P K, Yu M Y, and Tsintsadze N L 1984 *Phys. Fluids* **27** 327
[3] Shukla N and Shukla P K 2007 *Phys. Lett. A* **367** 120
[4] Schwarz U T, English L Q and Sievers A J 1999 *Phys. Rev. Lett.* **83** 223
[5] Xie A H, van der Meer L, Hoff W and Austin R H 2000 *Phys. Rev. Lett.* **84** 5435
[6] Fleischer J W, Segev M, Efremidis N K and Christodoulides D N 2003 *Nature* **422** 147
[7] Sen S, Hong J, Bang J, Avalos E and Doney R 2008 *Phys. Rep.* **462** 21
[8] Rosas A and Lindenberg K 2018 *Phys. Rep.* **735** 1
[9] Korteweg D J and de Vries G 2011 *Philos. Mag.* **91** 1007
[10] Nesterenko V F 1983 *J. Appl. Mech. Tech. Phys.* **24** 733
[11] Nesterenko V F 2018 *Phil. Trans. R. Soc. A* **376** 20170130
[12] Fermi E, Pasta J and Ulam S 1974 *Lect. Appl. Math.* **15** 143
[13] Vainchtein A 2022 *Phys. D* **434** 133252
[14] Nesterenko V F 2001 *Dynamics of Heterogeneous Materials* (New York: Springer-Verlag) pp. 17–20
[15] Sen S, Manciu M and Wright J D 1998 *Phys. Rev. E* **57** 2386
[16] Sen S and Manciu M 1999 *Phys. A* **268** 644
[17] Manciu M, Sen S and Hurd A J 1999 *Phys. A* **274** 588
[18] Chong C, Porter M A, Kevrekidis P G and Daraio C 2017 *J. Phys.: Condens. Matter* **29** 413003
[19] Manciu M, Sen S and Hurd A J 2000 *Phys. Rev. E* **63** 016614
[20] Manciu F S and Sen S 2002 *Phys. Rev. E* **66** 016616
[21] Avalos E and Sen S 2009 *Phys. Rev. E* **79** 046607
[22] Wen Z Y, Wang S J, Zhang X M and Lei L 2007 *Chin. Phys. Lett.* **24** 2887
[23] Santibanez F, Munoz R, Caussarieu A, Job S and Melo F 2011 *Phys. Rev. E* **84** 026604
[24] Shen Y, Kevrekidis P G, Sen S and Hoffman A 2014 *Phys. Rev. E* **90** 022905
[25] Wang F G, Yang Y Y, Han J F and Duan W S 2018 *Chin. Phys. B* **27** 044501
[26] Wu Q Q, Liu X Y, Jiao T F, Sen S and Huang D C 2020 *Chin. Phys. Lett.* **37** 074501
[27] Zhang W and Xu J 2021 *Int. J. Mech. Sci.* **191** 106073
[28] Tichler A M, Gomez L R, Upadhyaya N, Campman X, Nesterenko V F and Vitelli V 2013 *Phys. Rev. Lett.* **111** 048001
[29] Liu S W, Yang Y Y, Duan W S and Yang L 2015 *Phys. Rev. E* **92** 013202
[30] Du W Q, Yang Y Y, Han J F and Duan W S 2020 *Indian J. Phys.* **94** 1249
[31] Yang Y Y, Liu S W, Yang Q, Zhang Z B, Duan W S and Yang L 2016 *AIP Advances* **6** 075317
[32] Su C H and Mirie R M 1980 *J. Fluid Mech.* **98** 509
[33] Chen Y S and Yeh H 2014 *J. Fluid Mech.* **749** 577
[34] Tong C, Shao Y L, Hanssen F C W, Li Y, Xie B and Lin Z L 2019 *Wave Motion* **88** 34
[35] Chambarel J, Kharif C and Touboul J 2009 *Nonlin. Processes Geophys.* **16** 111
[36] Deng G, Biondini G and Sen S 2020 *Chaos* **30** 043101
[37] Maxworthy T 1976 *J. Fluid Mech.* **76** 177
[38] Fenton J D and Rienecker M M 1982 *J. Fluid Mech.* **118** 411
[39] Power H and Chwang A T 1984 *Wave Motion* **6** 183
[40] Byatt-Smith J G B 1988 *J. Fluid Mech.* **197** 503
[41] Cooker M J, Weidman P D and Bale D S 1997 *J. Fluid Mech.* **342** 141
[42] Chen Y Y, Kharif C, Yang J H, Hsu H C, Touboul J and Chambarel J 2015 *Eur. J. Mech. B Fluid.* **49** 20
[43] Zhang J, Yang Y, Xu Y X, Yang L, Qi X and Duan W S 2014 *Phys. Plasmas* **21** 103706
[44] Qi X, Xu Y X, Duan W S, Zhang L Y and Yang L 2014 *Phys. Plasmas* **21** 082118
[45] Zhang J, Qi X, Zhang H and Duan W S 2016 *Chin. Phys. Lett.* **33** 065202
[46] Landau L D and Lifshitz E M 2011 *Theory of Elasticity* (5th edn.) (Beijing: Higher Education Press) pp. 30–35
[47] Daraio C, Nesterenko V F, Herbold E B and Jin S 2005 *Phys. Rev. E* **72** 016603
[48] Nesterenko V F 1994 *J. Phys. IV* **4** C8–729
[49] Nesterenko V F, Lazaridi A N and Sibiryakov E B 1995 *J. Appl. Mech. Tech. Ph+* **36** 166
[50] Daraio C, Nesterenko V F and Jin S 2004 *AIP Conf. Proc.* **706** 197
[51] Job S, Melo F, Sokolow A and Sen S 2007 *Granular Matter* **10** 13
[52] Byatt-Smith J G B 1971 *J. Fluid Mech.* **49** 625
[53] Whitham G B 2016 *Linear and Nonlinear Waves* (Beijing: Science Press) pp. 438–444
[54] Craig W, Guyenne P, Hammack J, Henderson D and Sulem C 2006 *Phys. Fluids* **18** 057106